ENERGY MATERIALS & THERMOELECTRICS

Reversible control of the electronic density of states at the Fermi level of $Ca_3Co_4O_{9+\delta}$ misfit-layered oxide single crystals through O^+/H^+ plasma exposure

D. Moser · M. G. Garnier · L. Karvonen · A. Shkabko · P. Aebi · A. Weidenkaff

Abstract Misfit-layered $Ca_3Co_4O_9$ crystals were grown and characterized via XRD, SEM, and photo-emission spectroscopy (PES). The evolution of the intensity at the Fermi level (E_F) with varying oxygen content was studied by PES. Oxygen species were successfully introduced and removed through O^+ and H^+ microwave-plasma (2.45 GHz, 2–5 mbar) treatments, respectively. A 5 min O^+ plasma exposure was observed to result into a drastic enhancement in the E_F intensity, demonstrating the influence of oxygen content to the charge carrier population in layered cobalt-oxide materials.

Introduction

Layered cobalt oxides have received much attention over the past 30 years. The initial focus of the research was on the low-temperature (electro-) chemical intercalation/deintercalation reactions, the results of which laid the foundation to the extensive Li-ion battery industry of present days [1]. In 1997, a combination of a high positive value of the thermoelectric power (Seebeck) coefficient ($S_{300 K} = dV/dT = 100$ μV/K) and low electrical resistivity ($\rho_{300 K} = 200$ μΩ cm)—unusual for an oxide material—was

D. Moser · L. Karvonen · A. Shkabko · A. Weidenkaff (✉)
Laboratory for Solid State Chemistry and Catalysis, Department of Mobility, Energy and Environment, EMPA-Swiss Federal Laboratories for Materials Science and Technology, Überlandstrasse 129, 8600 Dübendorf, Switzerland
e-mail: anke.weidenkaff@empa.ch

M. G. Garnier · P. Aebi
Département de Physique and Fribourg Center for Nanomaterials, Université de Fribourg, 1700 Fribourg, Switzerland

discovered from $Na_{0.5}CoO_2$ [2]. A sequence of similar observations across the layered cobalt-oxide family, particularly among the misfit-layered cobalt oxides, such as $Ca_3Co_4O_{9+\delta}$ [3] and $Bi_2Sr_2Co_2O_x$ [4], took place over the decade following this first observation. The realization of a superconductive state in $Na_{0.3}CoO_2 \cdot 1.3H_2O$ ($T_c = 4.2$) oxyhydrate phase in the year 2004 [5] further emphasized the role of layered cobalt-oxide compounds as highly interesting electron systems.

Many of the properties of the layered cobalt oxides can be understood on the basis of their anisotropic crystal structure. The basic structural component is the metallic conductive $[CoO_2]$ layer-block (Fig. 1), presenting a hexagonally close-packed CdI_2-type crystal structure. The negatively charged $[CoO_2]$ layer-blocks are linked together by positively charged electrically insulating intermediate layer-blocks, consisting either of a single plane of electropositive cations or two to four planes of cations and oxide anions arranged into a distorted rock-salt-type metal-oxide structure. The different chemical reactivity of the layer-blocks together with the weak inter-block binding forces, lowered even further in misfit-layered materials [6], enable the selective adaptability of the intermediate layer-block to mildly reactive conditions while still conserving the $[CoO_2]$ layer-block [7, 8]. The electrical transport between the separated $[CoO_2]$ sheets also becomes suppressed due to the loose inter-block bonding, resulting into a strongly correlated two-dimensional electron system [2]. The main reason for the high thermoelectric performance, according to prevailing understanding, is the charge-carrier entropy enhancement provided by the elevated spin entropy of the formally four-valent cobalt species in the $[CoO_2]$ layer-block embedded among the matrix of trivalent cobalt species [9]. In order to perform a more concrete analysis over the electronic band structures of these

Fig. 1 An idealized model of $Ca_3Co_4O_{9+\delta}$ ([Ca_2CoO_3]$_{0.62}CoO_2$) misfit-layered oxide. Due to the mismatch of the b parameters of CoO_2 (H) and Ca_2CoO_3 (RS) sublattices (b_H/b_{RS} = irrational number), the idealized unit cell, schematized in the figure, is extended in the b direction in a real structure

materials close to the Fermi level (E_F) and to understand their influences to the transport properties, photoemission spectroscopy (PES) is the technique of choice.

The reported PES studies in the layered cobalt-oxide family, up to date, have concentrated on the A_xCoO_2 system (A = Na, K, Rb; $0.33 < x < 0.77$) [10–28]. The main focus has been on validating the earlier theoretical band-structure calculation results applying LDA + U approximation and predicting the Fermi surface to host a large hexagonal a_g hole pocket at a high-symmetry Γ point of the hexagonal Brillouin zone surrounded by six smaller e_g hole pockets at each of the K points [29]. While the pocket around the Γ point appears to be a general feature in the layered cobalt-oxide family, characteristic for the hexagonal [CoO_2] layer-block, the pockets around the K points remain undetected [27, 30]. The proposed reasons for the absence of the latter have currently been understood as a result of enhanced electron-correlation effects and/or an A-cation disorder [31, 32]. Much less studies exist for the misfit-layered family [30, 33–35]. A general conclusion about the reasons for the high S is the a_g hole pocket representing a flat electron band that only slightly crosses the E_F.

This work focuses on the $Ca_3Co_4O_{9+\delta}$ misfit-layered oxide. As described by the more elaborate chemical formula, [Ca_2CoO_3]$_{0.62}$[CoO_2] [36], the structure comprises

hexagonal [CoO_2] layer-blocks (H) sandwiching rock-salt type [Ca_2CoO_3] layer-blocks (RS), as demonstrated in Fig. 1. The structure can, therefore, be considered as an intergrowth of two crystal structures with misfit lattice parameters along the b-axis direction. The compound also presents a wide oxygen non-stoichiometry range, affecting the character and degree of electrical conductivity, which is generally more metallic at higher oxygen contents, thus resembling more the transport characteristics expected for the [CoO_2] layer-block [37]. Our results highlight the effect of oxygen addition to the band structure in the proximity to E_F. In this study, PES measurements coupled with oxidizing/reduction treatments were performed to study the influence of oxygen content on the electronic band structure close to the E_F in a $Ca_3Co_4O_{9+\delta}$ misfit-layered cobalt oxide.

Experimental

Single crystals of $Ca_3Co_4O_{9+\delta}$ were grown using a molten-salt flux method. Polycrystalline $Ca_3Co_4O_{9+\delta}$ powder was first synthesized through a solid-state reaction. A stoichiometric mixture of Co_3O_4 (99.7 %) and $CaCO_3$ (99.5 %) was prepared and calcined at 1173 K in air for 20 h with one intermittent pelletizing and re-grinding. 0.5 g (2.5 wt%) of the as-synthesized $Ca_3Co_4O_{9+\delta}$ polycrystalline powder was then mixed into 20 g of K_2CO_3:KCl flux, prepared in 4:1 molar proportions. The $Ca_3Co_4O_{9+\delta}$/K_2CO_3/KCl mixture was placed into a conically shaped 100 ml corundum crucible (60 mm inner diameter and 56 mm height) and covered with a corundum lid. The temperature program of the re-crystallization process was carried out in a muffle furnace proceeded through heating of the mixture up to 1163 K with a rate of 5 K/min, followed by dwelling the molten-salt solution at 1163 K for 10 h and a subsequent slow cooling down to 973 K at a rate of 2 K/h, after which the furnace was switched off and let spontaneously to cool down to room temperature. The as-grown $Ca_3Co_4O_{9+\delta}$ crystals were separated from the flux using 0.1 M HNO_3(aq.), followed by a wash with distilled water and drying in air at 363 K for 5 h.

Powder X-ray diffraction (XRD) data were recorded for the as-crystallized $Ca_3Co_4O_{9+\delta}$ materials with a PANalytical X'Pert Pro MPD diffractometer using Bragg–Brentano (θ–2θ) geometry, Cu-K$_{\alpha 1}$ radiation (1.5405 Å, filtered with Johansson monochromator using Ge(111) crystal), and an X'Celerator line detector.

The photoemission data were collected using an upgraded SCIENTA SES 2002 spectrometer, equipped with an X-ray source (Mg–K$_\alpha$: 1253.6 eV) and a monochromatized UV source (He I: 21.2 eV; He II: 40.8 eV) with energy resolutions 1 eV and 5 meV, respectively. The

X-ray photoemission (XPS) was used for detecting the chemical species present in the sample. The UV source was used for the in-detail observation of the shallow electron bands close to E_F. The angle-resolved valence-band spectra were measured from a delaminated $Ca_3Co_4O_{9+\delta}$ crystal surface using the He II line excitation and an electron-analyzer mode that records the intensity of the photoelectron flux at a chosen binding energy (B.E.) value with respect to the escape angle. Under certain assumptions, the escape angle of a photoelectron can be related to the wave vector of the initial-state electron hosted by the relaxed band structure [38]. Based on the collected data, together with the lattice parameters [39], a picture of the electron dispersion relation, $E(k)$, can then be produced. The effect of oxidation and reduction of the sample surface on the E_F was further studied using consecutive treatments with O^+ or H^+ plasma. The microwave discharge plasma (2.45 GHz) used in the treatments was produced in a separate chamber filled with O_2- or H_2-gas (2–5 mbar) directly connected to the photoemission measurement chamber. The average kinetic energy of the ions in the plasma has been determined, using a home-made ion detector application, to be around 5 eV. After the plasma treatment, a pumping time of some minutes was enough to recover the vacuum adequately to perform the photoemission measurement. E_F-focused spectral data were collected after each exposure using He I line excitation.

The shortcoming of PES, especially with samples that require an *ex-situ* preparation, is the extreme surface sensitivity (typically 20 Å for XPS and 10 Å for UV photoemission (UPS)). Therefore, the sample surface has to be thoroughly cleaned before the measurement, as it may have been contaminated by the surrounding atmosphere during the transfer between the sample synthesis and the analytical setups. The strongly anisotropic structure of $Ca_3Co_4O_{9+\delta}$ consisting of loosely interacting layers enabled us to create fresh sample surfaces through delamination of the upper crystal layers with adhesive tape. Such a delamination procedure is possible directly under ultra-high vacuum conditions inside the photoemission analysis chamber.

Results and discussion

The product of the re-crystallization experiments from molten salt consisted of plate-like particles with up to 3×3 mm^2 lateral dimensions. The XRD pattern recorded from a single sample platelet, with its flat surface parallel to the sample-holder surface, is shown in Fig. 2a. All the observed reflections matched with the ($00l$) reflections of the $Ca_3Co_4O_{9+\delta}$ reference pattern [40] while the reflections with h and $k \neq 0$ remained absent, indicating a complete c-axis alignment of the single-crystalline domains

perpendicular to the flat surfaces of the platelet. A scanning electron microscopy (SEM) image (Fig. 2b), taken along the flat side of the crystal reveals the exfoliating behavior of the re-crystallized product leading into formation of thin lamellar crystalline sheets of ~ 0.1 μm thickness.

The overview PES spectrum is shown in Fig. 3a. In addition to the expected features from Ca, Co, and O related species, rather intensive features provided by carbon (B.E. $= -284$ eV (C 1 s) and -970 eV (C KLL)) are observable. It appears that the carbon, originating from the K_2CO_3-based crystallization flux (yet difficult to remove completely), is not contained within the $Ca_3Co_4O_{9+\delta}$ structure itself but is present only on the surfaces of the ~ 0.1 μm thick leaf-like crystal sheets exfoliating from the larger as-crystallized crystal body (Fig. 2b). Despite the carbonaceous residuals, good-quality cleaved surfaces were achieved, as is demonstrated in Fig. 3b by the low-energy electron diffraction (LEED) pattern. The sixfold symmetry of the pattern further suggests that the sample-crystal surface is terminated by the hexagonal [CoO_2] layer. The He II valence-band spectrum of $Ca_3Co_4O_{9+\delta}$ is shown in Fig. 3c. Comparing this spectrum with the previously published ones [33] and using the tabulated cross sections and binding energies [41] one can attribute the peak at -25 eV to Ca 3p, while the two higher-energy peaks, at about -5 and -1.5 eV, feature mostly O 2p character with a small Co 3d contribution. The peak around -10 eV is of less clear origin, but could be a correlation satellite due to strong on-site Coulomb interactions, as interpreted in the case of an analogous feature in the PES spectrum of the closely related $Na_{0.7}CoO_2$ by Kuprin et al. [12].

The angular-dispersion spectrum of the sharp -1.5 eV valence-band peak in the proximity of the E_F is presented in Fig. 4. The oscillatory behavior with a periodicity related to the Γ–M distance has also been reported by Takeuchi et al. [30]. However, the position of the valence band in their case is closer to E_F. Additionally, they see another weak band crossing E_F which is absent in our case. Even if in their data this band is not very intense, as apparently the second derivative of the data is needed to evidence it, the absence in our case despite the presence of the LEED pattern and the angular-dispersion spectrum, indicating good sample quality, is probably an effect of carbon at the surface. The difference in position of the valence band might also be due to this supplementary carbon (see below).

The effects of the oxidizing/reducing plasma exposures were observed through the change of the -1.5 eV valence-band peak, the initial appearance of which is shown in Fig. 5(i). A 1 min exposure to O^+ plasma (Fig. 5(ii)) shifts the feature toward lower B.E. (i.e., closer to the position as observed by Takeuchi et al.), together with an enhancement

Fig. 2 a XRD pattern of the highly oriented $Ca_3Co_4O_{9+\delta}$ single crystal re-crystallized using K_2CO_3/KCl flux. b SEM image revealing the exfoliated structure of the re-crystallization product
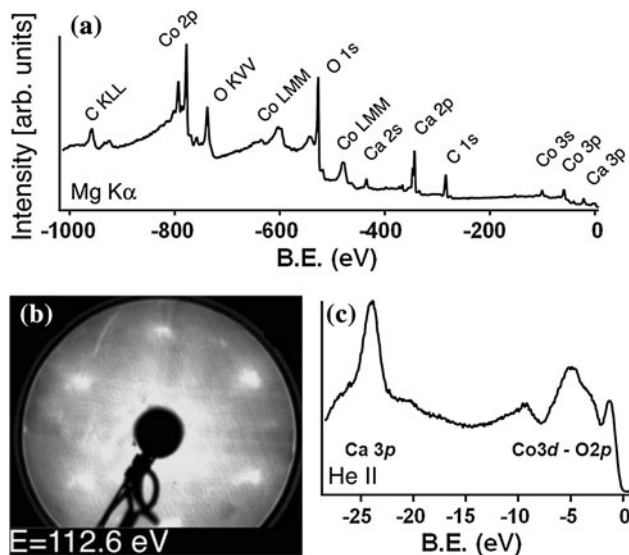

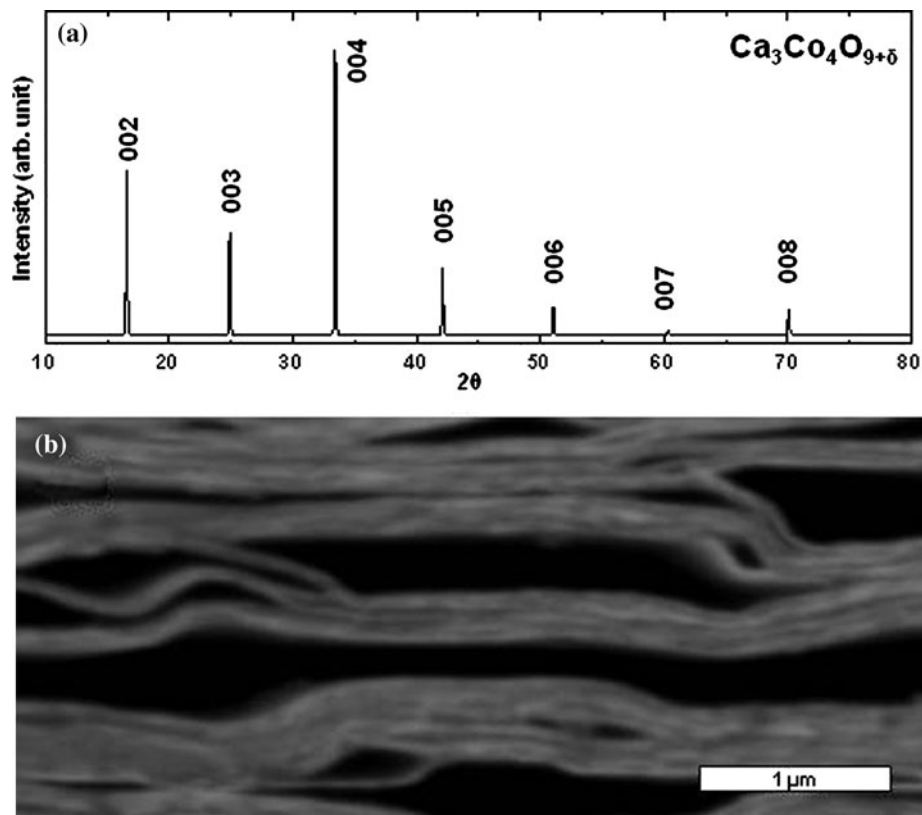Fig. 3 a XPS spectrum (Mg–K_α excitation: 1253.6 eV) recorded for detecting the chemical species present in the as-prepared $Ca_3Co_4O_{9+\delta}$ crystals. b LEED pattern (112.6 eV electron energy) recorded for verifying the single-crystallinity and c PES spectrum (He II excitation: 40.8 eV) recorded for observing the valence-band features on the $Ca_3Co_4O_{9+\delta}$ crystal surface

Fig. 4 Angular-dispersion PES spectrum (He II line excitation: 40.8 eV) over the B.E. region next to E_F on the $Ca_3Co_4O_{9+\delta}$ single-crystal surface

of the spectral intensity at E_F. A simultaneous change of the C 1s peak at B.E. = -284 eV (not shown here) was also observed. The dominant feature, consisting of two mutually 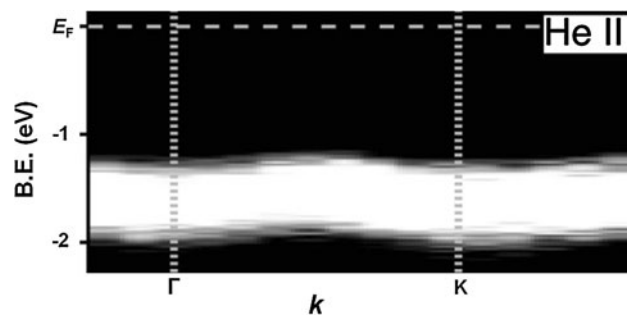merging features, is highly reduced by the plasma exposure, down to 30 % of its original spectral weight, revealing the reaction of the carbonaceous species with the O^+ ions and a subsequent removal from the sample surface. The other structures at higher B.E. presented no observable shifting behavior. Also interestingly, the oscillatory behavior of the dispersion featured in Fig. 4 was not affected, apart from the energy position of the band. A continued exposure of O^+ plasma (Fig. 5(iii)) leads to further positive shift of the -1.5 eV valence-band peak and an enhancement of the intensity at E_F, the saturation of the behavior being reached after 5 min exposure. A subsequent H^+ plasma exposure, eliminating the previously introduced oxygen species from the sample surface, reverses the
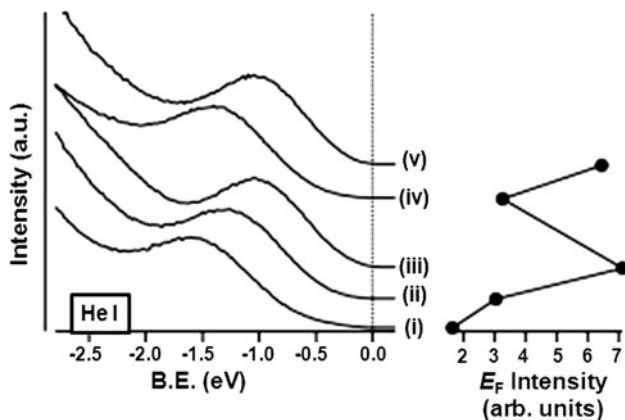
Fig. 5 *Left plot*: PES spectra (He I line excitation: 21.2 eV) over the B.E. region next to E_F measured on the $Ca_3Co_4O_{9+\delta}$ single-crystal surface after subsequent plasma treatments: (*i*) after delamination, (*ii*) after 1 min. O^+ plasma exposure, (*iii*) after 5 min. of O^+ plasma exposure, (*iv*) after 5 s. of H^+ plasma exposure and (*v*) after 1 min. of O^+ plasma exposure. *Right plot*: corresponding relative spectral intensities at E_F

behavior providing a negative shift of the peak close to its initial B.E. together with a lowering intensity at E_F (Fig. 5(iv)). Reversibility of the process was further confirmed by reintroduction of the positive shift and E_F intensity enhancement by a renewed 1 min exposure to O^+ plasma (Fig. 5(v)). The corresponding transport data measured on the oxygen content varied polycrystalline misfit-layered oxides [37] display a significant reduction of resistivity with oxygen excess and improvement of the thermopower, which is in a good correlation with the change in intensity at E_F observed in our study. Indeed, the intensity at E_F is a measure for the available charge carriers and, therefore, a higher intensity is indicative for a lower resistivity.

Conclusions

Crystals of the $Ca_3Co_4O_{9+\delta}$ misfit-layered oxide were grown by a K_2CO_3/KCl molten-salt flux method. The as-crystallized platelet-shaped material exhibited large flat surfaces parallel to the *a-b* crystal axes. The tendency of the as-grown crystals to exfoliate along the *c* axis facilitates generation of smooth surfaces required for PES measurements. Despite the presence of residual carbon species at the surface, a LEED pattern could be observed together with a dispersive band. The evolution of the spectral intensity at E_F with varying oxygen content on the flat surfaces of the crystals was studied through PES. Oxygen species were successfully introduced and removed through O^+ and H^+ microwave-plasma treatments, respectively. A strong variation of spectral intensity at E_F was detected

with O implantation. The variation reversibly depends on the oxygen content. The observation underlines the significance of oxygen-assisted hole-doping as means of tuning the number of charge carriers at E_F in the material.

References

1. Mizushima K, Jones PC, Wiseman PJ, Goodenough JB (1980) Mater Res Bull 15:783
2. Terasaki I, Sasago Y, Uchinokura K (1997) Phys Rev B 56(20):R12685
3. Miyazaki Y, Kudo K, Akoshima M, Ono Y, Koike Y, Kajitani T (2000) Jpn J Appl Phys 39:L531
4. Funahashi R, Matsubara I, Sodeoka S (2000) Appl Phys Lett 76:2385
5. Takada K, Sakurai H, Takayama-Muromachi E, Izumi F, Dilanian RA, Sasaki T (2003) Nature 422(6927):53
6. Yamauchi H, Karvonen L, Egashira T, Tanaka Y, Karppinen M (2011) J Solid State Chem 184:64
7. Karppinen M, Asako I, Motohashi T, Yamauchi H (2005) Phys Rev B 71:092105
8. Cushing BL, Wiley JB (1998) J Solid State Chem 141:385
9. Koshibae W, Tsutsui K, Maekawa S (2000) Phys Rev B 62(11): 6869
10. Arakane T, Sato T, Takahashi T, Ding H, Fujii T, Asamitsu A (2007) J Phys Soc Jpn 76(5):054704
11. Hasan MZ, Qian D, Foo ML, Cava RJ (2006) Ann Phys-N Y 321(7):1568
12. Kuprin AP, Hasan MZ, Chuang YD, Qian D, Foo M, Cava RJ (2006) J Phys Chem Solids 67(1–3):235
13. Usui H, Iwasawa H, Hirose M et al (2010) Phys C 470:S758
14. Arakane T, Sato T, Takahashi T, Fujii T, Asamitsu A (2007) Phys C 463–465:149
15. Hasan MZ, Qian D, Foo M, Cava RJ (2007) Phys C 460–462:186
16. Arakane T, Sato T, Takahashi T, Fujii T, Asamitsu A (2011) New J Phys 13(4):043021
17. Yang HB, Wang Z, Ding H (2007) J Phys-Condens Mater 19(35):355004
18. Arakane T, Sato T, Takahashi T, Fujii T, Asamitsu A (2009) Phys Rev B 80(8):081101
19. Yang HB, Wang SC, Sekharan AKP et al (2004) Phys Rev Lett 92(24):246403
20. Hasan MZ, Chuang YD, Qian D et al (2004) Phys Rev Lett 92(24):246402
21. Shimojima T, Yokoya T, Kiss T et al (2005) Phys Rev B 71(2): 020505
22. Yang HB, Pan ZH, Sekharan AKP et al (2005) Phys Rev Lett 95(14):146401
23. Qian D, Wray L, Hsieh D et al (2006) Phys Rev Lett 96(4): 046407
24. Qian D, Wray L, Hsieh D, Viciu L, Cava RJ, Luo JL, Wu D, Wang NL, Hasan MZ (2006) Phys Rev Lett 97(18):186405
25. Lee KW, Pickett WE (2007) Phys Rev B 76(13):134510
26. Pillay D, Johannes MD, Mazin II (2008) Phys Rev Lett 101(2008):246808
27. Arakane T, Sato T, Takahashi T, Fujii T, Asamitsu A (2010) Phys Rev B 81(11):115132
28. Takeuchi T, Kondo T, Takami T et al (2004) Phys Rev B 69(12):125410

29. Singh DJ (2000) Phys Rev B 61(20):13397
30. Takeuchi T, Kondo T, Kitao T, Soda K, Shikano M, Funahashi R, Mikami M, Mizutani U (2005) J Electron Spectrosc 144–147:849
31. Singh DJ, Kasinathan D (2006) Phys Rev Lett 97:016404
32. Shorikov A, Korshunov MM (2011) JETP Lett 93:80
33. Takeuchi T, Kondo T, Soda K, Mizutani U, Funahashi R, Shikano M, Tsuda S, Yokoya T, Shin S, Muro T (2004) J Electron Spectrosc 137–140:595
34. Kang JS, Han SW, Fujii T, Terasaki I, Lee SS, Kim G, Olson CG, Lee HG, Kim JY, Min BI (2006) Phys Rev B 74(20):205116
35. Valla T, Johnson PD, Yusof Z et al (2002) Nature 417(6889):627
36. Miyazaki Y, Onoda M, Oku T, Kikuchi M, Ishii Y, Ono Y, Morii Y, Kajitani T (2002) J Phys Soc Jpn 71(2):491
37. Moser D, Karvonen L, Populoh S, Trottmann M, Weidenkaff A (2011) Solid State Sci 13:2160
38. Hüfner S (2008), 3rd ednSpringer, Berlin
39. Miyazaki Y (2004) Solid State Ionics 172:463
40. Brisi C, Piero R (1968) Ann Chim 58:676
41. Yeh JJ, Lindau I (1985) Atom Data Nucl Data 32:1